Front. Mater. Sci. 2022, 16(4): 220617
https://doi.org/10.1007/s11706-022-0617-5

RESEARCH ARTICLE

Regulation effect of osteoblasts towards osteocytes by silk fibroin encapsulation

Dandan LUO[1,2,3], Rui ZHANG[1,2], Shibo WANG[1,2], M. Zubair IQBAL[1,2], Ruibo ZHAO (✉)[1,2], and Xiangdong KONG[1,2]

1 Institute of Smart Biomedical Materials, School of Materials Science and Engineering, Zhejiang Sci-Tech University, Hangzhou 310018, China
2 Zhejiang-Mauritius Joint Research Center for Biomaterials and Tissue Engineering, Zhejiang Sci-Tech University, Hangzhou 310018, China
3 School of Textile Science and Engineering, Zhejiang Sci-Tech University, Hangzhou 310018, China

ABSTRACT: Herein, the rational design micromilieus involved silk fibroin (SF)-based materials have been used to encapsulate the osteoblasts, forming an extracellular coated shell on the cells, which exhibited the high potential to shift the regulation of osteoblasts to osteocytes by encapsulation cues. SF coating treated cells showed a change in cell morphology from osteoblasts-like to osteocytes-like shape compared with untreated ones. Moreover, the expression of alkaline phosphatase (ALP), collagen I (Col I) and osteocalcin (OCN) further indicated a potential approach for inducing osteoblasts regulation, which typically accelerates calcium deposition and cell calcification, presenting a key role for the SF encapsulation in controlling osteoblasts behavior. This discovery showed that SF-based cell encapsulation could be used for osteoblasts behavior regulation, which offers a great potential to modulate mammalian cells' phenotype involving alternating surrounding cues.

KEYWORDS: cell encapsulation; silk fibroin; osteoblasts modulation; cell differentiation; cell calcification

Contents

Received June 1, 2022; accepted August 9, 2022

E-mail: rzhao@zstu.edu.cn

1 Introduction

Many living organisms in nature can construct envelopes to achieve self-protection and functionalization [1]. For example, diatom cells will secrete silicon mineralized proteins to the outside of the cell, enrich the silicon element in the water, and form a layer of ordered silicon shell outside the cell, improving its resistance to stress [2–4]. Biomimetic mineralization was used to develop the calcium phosphate (CaP) shell coating on organisms [5–6], which could boost the organism's ability to adapt to the threatening microenvironment [7]. When the encapsulation material was replaced with silicon dioxide (SiO_2) by silicon mineralization, the yeast's resistance to stress could be further improved [8], especially the high-temperature resistance of yeast cells significantly improved [9]. It demonstrated that materials encapsulation could significantly regulate cell behavior [10–13], providing great potential for developing living cell-based biomaterials.

Furthermore, the material coating layer will regulate the physiological milieus of the cell [14], which may endow cells with new functions. It confirmed that when the chlorella cells were aggregated by biomineralization, the inside chlorella could improve their production efficacy of H_2, contrary to the normal process of producing O_2 [15]. Moreover, encapsulating the Jurkat cell with titanium dioxide (TiO_2) could significantly trigger interleukin-2 (IL-2) secretion [16], demonstrating that the appropriate material to encapsulate the cells may achieve the functional differentiation and behavior transformation of cell functions [17–18].

Osteoblasts are generally sourced cell materials for bone tissue engineering due to their osteogenic differentiation potential towards osteocytes [19–21]. Currently, modulation of osteoblasts phenotype is still a significant challenge due to a milieu of cues *in situ* and high cost [22]. Strategies of encapsulating the osteoblasts may be a cue to induce their differentiation [23], which may be a facile alternative for cell-based hybrid materials. Silk fibroin (SF), as a central component of silk protein, has become one of the most attractive biomaterials with biocompatibility, low immunogenicity and elastic mechanical properties [24–25], which have demonstrated great cues for tissue engineering, especially for bone tissue [26–27]. More generally, the interaction between cells and silk materials could induce cell adhesion and proliferation [28–29], driving the differentiation of mesenchymal stem cells into bone cells [30–33], which followed an attractive hypothesis that SF might be an encapsulating cue to induce the osteoblasts towards osteocytes.

Herein, we prepared the encapsulated osteoblasts with SF using the electrostatic layer-by-layer encapsulation method and checked whether the coating could be used as a differentiation cue for osteoblasts regulation. Furthermore, the murine osteoblasts (MC3T3-E1) were used as the model cells, and the influences of coated treatment for cell differentiation and associated transformation were further detected, which gives us a new understanding of initial coating may be regarded as persisting cue for osteoblasts towards osteocytes.

2 Materials and methods

2.1 Materials

Na_2CO_3 (Sigma-Aldrich, USA), poly(ethyleneimine) (PEI; molecular weight (MW) 10 000; 99%, Aldrich, Germany), phosphate-buffered saline (PBS; Hyclone, USA), α-minimal essential medium (α-MEM; Hyclone, USA), fetal bovine serum (FBS; Gibco, US), a penicillin–streptomycin solution (Biosharp, China), 0.25% trypsin-EDTA, a Cell Counting Kit-8 (CCK-8), 4% paraformaldehyde solution, triton X-100 and nuclei visualization solution 6-diamidino-2-phenylindole (DAPI), alkaline phosphatase (ALP) activity assay Kit, bicinchoninic acid (BCA) protein assay Kit (Beyotime, China), TRIzol® Plus RNA Purification Kit, rhodamine-phalloidin (Invitrogen, OR, USA), Live/Dead™ Viability/Cytotoxicity Kit (Life Technologies, US), a mouse anti-collagen I antibody (ab6308, Abcam, UK), a mouse anti-osteocalcin antibody (ab13420, Abcam), a rabbit anti-ALP antibody (ab83259, Abcam), an horseradish peroxidase (HRP)-labeled goat anti-mouse IgG (H + L) antibody (31160, Thermo Pierce) and an HRP-labeled goat anti-rabbit IgG (H + L) antibody (31210, Thermo Pierce) were used as received.

2.2 Extraction of SF

Extraction of SF was performed according to our previous protocol [34]. In brief, silkworm cocoons from *Bombyx*

mori were cut into small pieces (5 g) and then degummed by boiling in 0.5% (w/v) Na_2CO_3 (2 L) solution 3 times for 30 min each. The degummed silk fibers were dissolved in boiling distilled water for 20 min and dried overnight in an oven at 37 °C. The dried SF was then solubilized in boiling 42% (w/v) $CaCl_2$ solution at a concentration of 20% (w/v) for 10 min. The solution was dialyzed against distilled water over 3 d and left in a dialysis bag under an electric fan for 2 d to increase SF concentration by water evaporation. The solution was centrifuged at 10 000 r·min^{-1} for 30 min at 4 °C to remove insoluble fibers. The concentration of silk solution was determined by weighing a known sample volume before and after drying overnight at 60 °C.

2.3 MC3T3-E1 cell culture and coating treated on cell surface

Mouse osteoblastic MC3T3-E1 cells were obtained from the cell bank of the Chinese Academy of Sciences (Shanghai, China). Cells were cultured in α-MEM supplemented with 10% FBS and 1% Pen-Strep antibiotic solution, incubated at 37 °C and humidified 5% CO_2 environment. Cells within 3–7 passages were used for further preparation of SF coating.

As for the SF coating process, MC3T3-E1 cells were firstly incubated in 50 μg·mL^{-1} solution of PEI in α-MEM medium without FBS at a density of 1×10^6 cells·mL^{-1} for 10 min under gentle pipetting after trypsin digestion and centrifugation. Then, the cells were incubated in 2 mg·mL^{-1} solution of SF for 10 min. After incubation, the cells were washed with α-MEM medium and separated by centrifugation (1000 r·min^{-1}, 3 min). After the above layer-by-layer steps of PEI and SF incubation 1–3 times, coated MC3T3-E1 cells were obtained.

2.4 Characterization of coated MC3T3-E1 cells

To determine the surface zeta potential of coated MC3T3-E1 cells, cells were suspended in PBS buffer at a density of 2×10^5 cells·mL^{-1} and measured with a Zetasizer analyzer (Zetasizer Nano ZS, UK).

The coated MC3T3-E1 cells were visualized by a brightfield microscope. Then, the coated MC3T3-E1 cells were fixed in 2.5% glutaraldehyde solution for 30 min at room temperature (RT), washed with PBS and deionized water (DI water), and dehydrated using a series of 30%, 50%, 60%, 70%, 80%, 90%, 95%, and 100% (v/v) ethanol solutions. The coated cells were further observed by field-emission scanning electron microscopy (FE-SEM, JSM-6500F, JEOL, Japan).

SF was fluorescently labeled with fluorescein isothiocyanate (FITC) to visualize the SF coating on the cells' surface. Briefly, 10 mg of FITC was dissolved in 100 mL of sodium carbonate-bicarbonate buffer at a concentration of 1 mol·L^{-1} (pH 10.0), and then 500 mg of SF was added. The mixture was stirred for 12 h at RT and then dialyzed in 3.5 kDa dialysis membranes, after which the solutions were lyophilized to obtain FITC-labeled SF (SF-FITC). MC3T3-E1 cells were coated with SF-FITC and observed using confocal laser scanning microscopy (CLSM; IX81-FV1000, Olympus, Japan).

2.5 Cell viability assay

The cytotoxicity of SF and PEI were evaluated by the CCK-8 method after MC3T3-E1 cells co-culture for 24 h at various concentrations. Coating treated MC3T3-E1 cells were stained with Live/Dead^{TM} Viability/Cytotoxicity Kit and imaged before and after culture for 14 d with the CLSM. As for cell viability, the coating treated cells were seeded in the 24-well plate at a cell density of 2×10^3 cells·mL^{-1} and cultured in the α-MEM growth medium for 14 d. At the predetermined time, the viability of cells cultured for various times up to 14 d was measured by CCK-8. Untreated MC3T3-E1 cells were used as a control.

2.6 Cell differentiation and cell morphology observation

To evaluate the osteoblastic formation ability of coating treated MC3T3-E1 cells after the SF encapsulation, cells were seeded in 6-well plates at a density of 1×10^5 cells per well in the α-MEM growth medium for 3 d. Then the cells were cultured in a differentiation medium with an osteogenic induction supplement (OS, 50 μg·mL^{-1} L-ascorbic acid, 10 mmol·L^{-1} sodium β-glycerophosphate, and 10 nmol·L^{-1} dexamethasone) for 3, 7, 14, and 21 d. Untreated MC3T3-E1 cells cultured without the OS were used as a control.

To observe the morphology of coated MC3T3-E1 cells cultured in the differentiation medium, rhodamine-phalloidin/DAPI staining was taken. Cells differentiated for 7 d were fixed with 4% paraformaldehyde for 10 min and then permeabilized with 0.5% (v/v) Triton X-100 for 5 min. The cytoskeleton was stained with rhodamine-phalloidin for 30 min followed by counterstaining with

DAPI to visualize the nuclei. Finally, the staining cells were observed with the CLSM.

The osteoblastic formation ability of coated MC3T3-E1 cells was evaluated by measuring ALP activity using the ALP activity assay Kit and BCA protein assay Kit. All the results were normalized with the total protein amount.

2.7 Quantitative PCR (qPCR)

After 14 d of culture in the differentiation medium, coating treated MC3T3-E1 cells were collected, and total RNA was extracted using TRIzol® Plus RNA Purification Kit (Invitrogen). SuperScript™ III First-Strand Synthesis SuperMix for qPCR (Invitrogen) was used for reverse transcription. The mRNA expression levels of ALP, collagen type I (Col I) and osteocalcin (OCN) were measured with Power SYBR® Green PCR Master Mix (Applied Biosystems, US). The primer sequences are listed in Table 1.

2.8 Western blot

The coating treated MC3T3-E1 cells differentiated for 14 d were washed twice with PBS and then lysed by 60 μL of lysis buffer with 1 mmol·L^{-1} phenylmethane sulfonyl fluoride (PMSF) for 30 min on ice. Total protein was acquired after centrifuging at 12000 r·min^{-1} at 4 °C for 5 min, and the concentration of protein was determined by the BCA protein assay Kit. The total soluble protein was separated on sodium dodecyl sulfate polyacrylamide gel electrophoresis (SDS-PAGE) and then transferred to the nitrocellulose membrane. After incubation in primary rabbit anti-ALP antibody (ab83259, Abcam) at 1:500, mouse anti-Col I antibody (ab6308, Abcam, UK) at 1:500, a mouse anti-OCN antibody (ab13420, Abcam) at 1:1000 dilutions, respectively, the secondary antibody HRP-labeled goat anti-rabbit IgG (H + L) antibody (31210, Thermo Pierce) and HRP-labeled goat anti-mouse IgG (H + L) antibody (31160, Thermo Pierce) at 1:500 dilutions in succession, the specific blot was visualized using enhanced chemiluminescence substrate (Tanon5500, Shanghai, China).

2.9 Alizarin red S (ARS) staining

ARS staining was performed to detect the calcium deposition from differentiated cells. Briefly, after differentiating for 21 d, the coating treated MC3T3-E1 cells were rinsed with PBS and incubated with 1% ARS solution for 30 min at RT. Then, the staining cells were gently washed with DI water and observed under a brightfield microscope.

2.10 Statistical analysis

All quantitative results are depicted as the mean ± standard deviation (SD). Statistical analysis was performed by analysis of *T*-test. The difference was considered statistically significant for a value of * $p < 0.05$, ** $p < 0.01$, and *** $p < 0.001$.

3 Results and discussion

3.1 Preparation and characterization of coated MC3T3-E1 cells

Inspired by layer-by-layer encapsulation, we fabricated an SF coating on osteoblasts' surfaces by a positive inducer PEI [35] (Fig. 1). It indicated that cocultured with SF at various concentrations (from 15 μg·mL^{-1} to 2 mg·mL^{-1}), the MC3T3-E1 cell maintained its high viability at 24 h (Fig. 2(a)), which was consistent with the results of the previous study [34]. PEI was used as a positive inducer

Table 1 qPCR primers

Gene	Genbank accession	Primer sequences (5' to 3')
Mouse GAPDH	GU214026.1	GAAGGTCGGTGTGAACGGATTTG
		CATGTAGACCATGTAGTTGAGGTCA
Mouse ALP	NM_007431.2	ACCTGACTGACCCTTCGCTCT
		CAATCCTGCCTCCTTCCACCA
Mouse Col I	NM_007743.2	CCTTCTGGACCCGTTGGCAAAGAT
		GGCTACCCTGAGAACCACGAACA
Mouse OCN	NM_001032298.2	CGCTCTGTCTCTCTGACCTCACA
		CCTCCTGCTTGGACATGAAGGCTTT

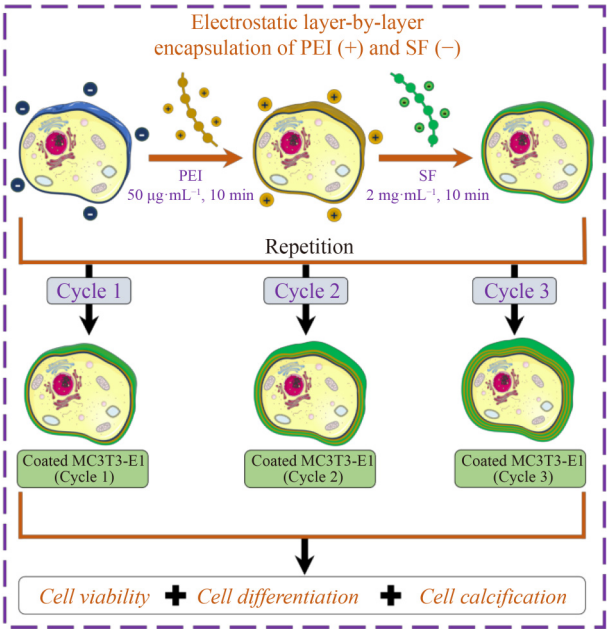

Fig. 1 Schematic showing electrostatic layer-by-layer encapsulation of PEI (+) and SF (−) on the negatively charged MC3T3-E1 cell surface. The cells treated after 1, 2, and 3 cyclic layer-by-layer encapsulation process (Cycles 1, 2, and 3) are denoted as coated MC3T3-E1 (Cycle 1), coated MC3T3-E1 (Cycle 2), and coated MC3T3-E1 (Cycle 3), respectively.

with biocompatibility for materials modification via electrostatic interaction [36], which could be absorbed onto the cells electrostatically. As observed in Fig. 2(b), although MC3T3-E1 cell viability was significantly reduced even cocultured with 5 μg·mL^{-1} of PEI at 24 h, no significant cytotoxicity was observed at 50 μg·mL^{-1} within 4 h (Fig. 2(c)). Therefore, 50 μg·mL^{-1} of PEI and 2 mg·mL^{-1} of SF were used for MC3T3-E1 encapsulation. The MC3T3-E1 cells suspension incubated in serum-free α-MEM medium containing 50 μg·mL^{-1} PEI for 10 min, then the cells were collected by centrifugation and followed by the incubation with the medium having 2 mg·mL^{-1} SF for 10 min.

As expected, the coated MC3T3-E1 cells could be achieved facilely. As shown in Fig. 2(d), the shift of zeta potential of cells from negative (MC3T3-E1, ~ −28.9 mV) to positive (MC3T3-E1@PEI, ~ +1.9 mV) and to negative (MC3T3-E1@PEI@SF, ~ −23.8 mV) showed the electrostatic layer-by-layer encapsulation process (Fig. 2(d)), suggesting the formation of cell coating. Indeed, the coatings were formed from a mixture of SF in the presence of PEI for a short period. From the brightfield and live/dead staining images, for the coated MC3T3-E1 (Cycles 1 and 2), either PEI or SF treatment showed no apparent influence on cellular morphology and viability compared with untreated cells. As for the cells in Cycle 3 treatment, the number of cells was slightly reduced, which may account for the cascade centrifugation. In addition, the cells remained alive after encapsulation, indicating that the coating treatment would not damage the cell viability (Figs. 2(e) and 2(f)).

After encapsulation, the surface of MC3T3-E1 cells was with a noticeable materials layer compared with the untreated cells (Fig. 3(a)). The surface of coated MC3T3-E1 (Cycle 1) cells with 1 layer and MC3T3-E1 (Cycle 2) with 2 layers of SF could demonstrate a smooth membrane-like coating. However, the coated MC3T3-E1 with 3 cycles were shrunken with fibers aggregating randomly on the cell surface. In addition, to identify the SF covered on cells, cells were coated by SF-FITC during the layer-by-layer encapsulation process [37]. Viewed with CLSM, the SF layer (green, labeled by FITC) was attached to the cell membrane (red, labeled by DiI), forming a shell-like structure (Fig. 3(b)). The coated MC3T3-E1 cells were detected for the FITC fluorescence signal, whereas no FITC signal was collected from the untreated MC3T3-E1 cells, further confirming the success of SF encapsulated cell.

3.2 Viability of coating treated MC3T3-E1

The coating treated MC3T3-E1 cells were cultivated in the α-MEM growth medium over 14 d for further investigation. At the predetermined time point, the viability of cells was evaluated by CCK-8 (Fig. 4(a)). The cell viability of the coating treated MC3T3-E1 (Cycle 1) and MC3T3-E1 (Cycle 2) cells was still over 80% as compared with control at 14 d, which indicated the high cell biocompatibility of the coating treatments of Cycles 1 and 2 process (Figs. 4(a)). However, the cell viability of coated MC3T3-E1 (Cycle 3) cells decreased significantly with cell viability at ~60% within 24 h and ~30% at 7 d, respectively (Figs. 4(a)). Viewed under a brightfield microscope, it was further confirmed that almost all of the encapsulated MC3T3-E1 cells with 1 and 2 layers of SF were still alive within 14 d, showing a comparable growth state and cell morphology with the untreated MC3T3-E1 group, while the coated MC3T3-E1 (Cycle 3) cells were all single without any cell pseudopodia and cell junction (Fig. 4(b)).

Besides, live/dead staining of the cells cultured for 14 d demonstrated that the viability of coated MC3T3-E1

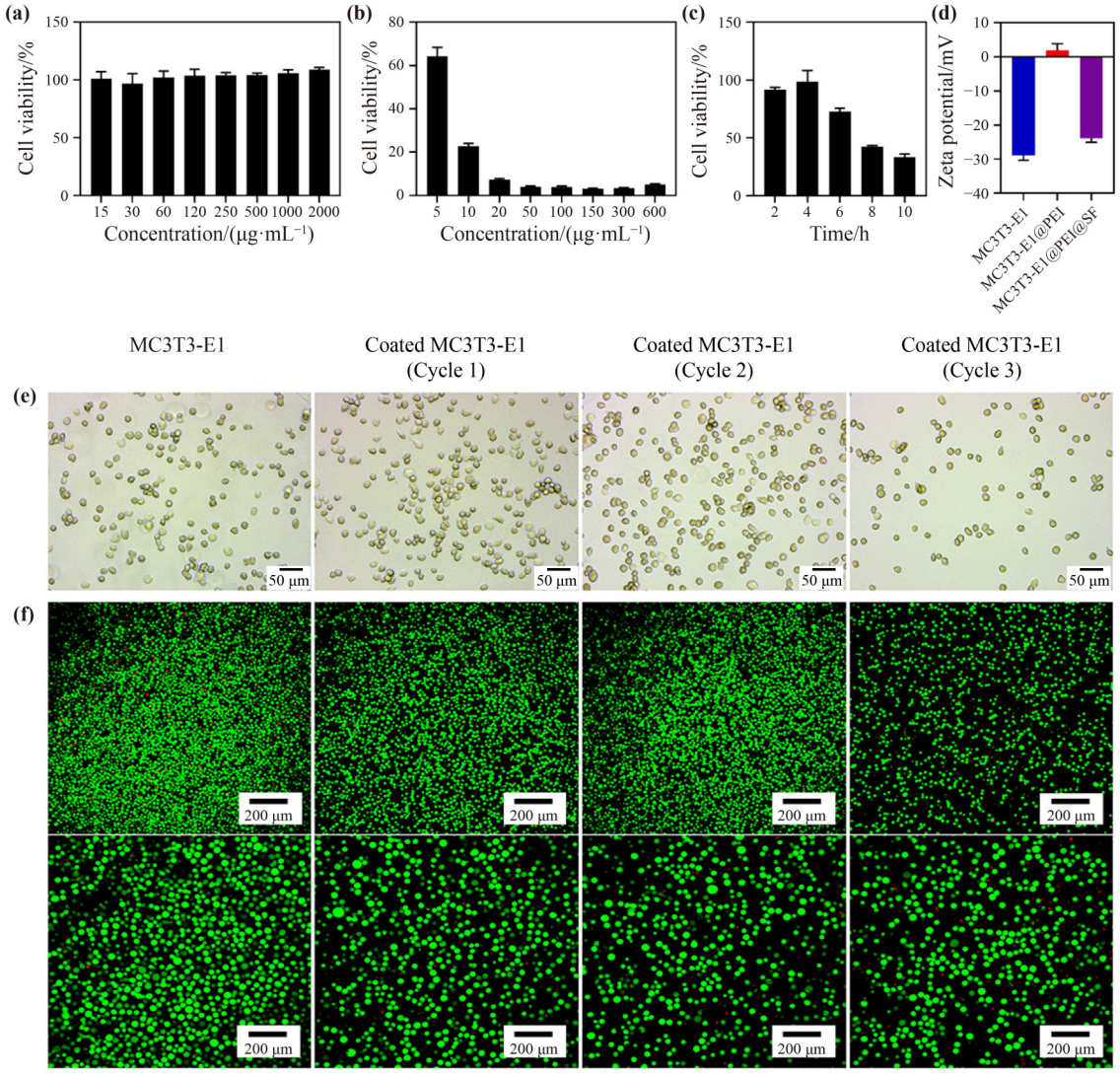

Fig. 2 Preparation of coating treated MC3T3-E1 cells. Cell viability of MC3T3-E1 after co-culture with various concentrations of (**a**) SF and (**b**) PEI for 24 h. (**c**) Cell viability of MC3T3-E1 after co-culture with 50 μg·mL^{-1} of PEI for various times. (**d**) Zeta potentials of MC3T3-E1, MC3T3-E1@PEI (after PEI treatment) and MC3T3-E1@PEI@SF (after PEI and SF treatment). (**e**) Brightfield microscope observation and (**f**) live/dead staining images of MC3T3-E1 and coating treated MC3T3-E1 cells. Green: live cell; red: dead cell.

(Cycle 1) and coated MC3T3-E1 (Cycle 2) cells was comparable to that of the untreated MC3T3-E1 group (Fig. 4(c)). Nevertheless, as shown in Fig. 3, the coated MC3T3-E1 cells with triple treatments displayed a cell shrinkage state, suggesting decreased cell viability. As a result, only the red fluorescence showed in the live/dead staining images of the coated MC3T3-E1 (Cycle 3) cells, suggesting a high rate of cell death after Cycle 3 treatments (Fig. 4(c)). These results were further in accordance with the quantitative CCK-8 measurement results, which indicated effective controlling the number of coating layers could regulate cell viability, whether still alive or going to die. It demonstrated that the mineral coating could affect cell viability [17,38], which accounts for mammalian cells' extreme sensitivity to extra mineral coating matter. It should be noted that SF, as a soft material, showed biocompatibility as a coating material for cell encapsulation [39].

3.3 Differentiation of coating treated MC3T3-E1

The coating strategy has demonstrated great potential for cell function regulation [40]. MC3T3-E1, as a typical osteoblast, has the potential to differentiate towards osteocytes, and the coating treatment may affect cell behavior transformation [41–43]. Compared with

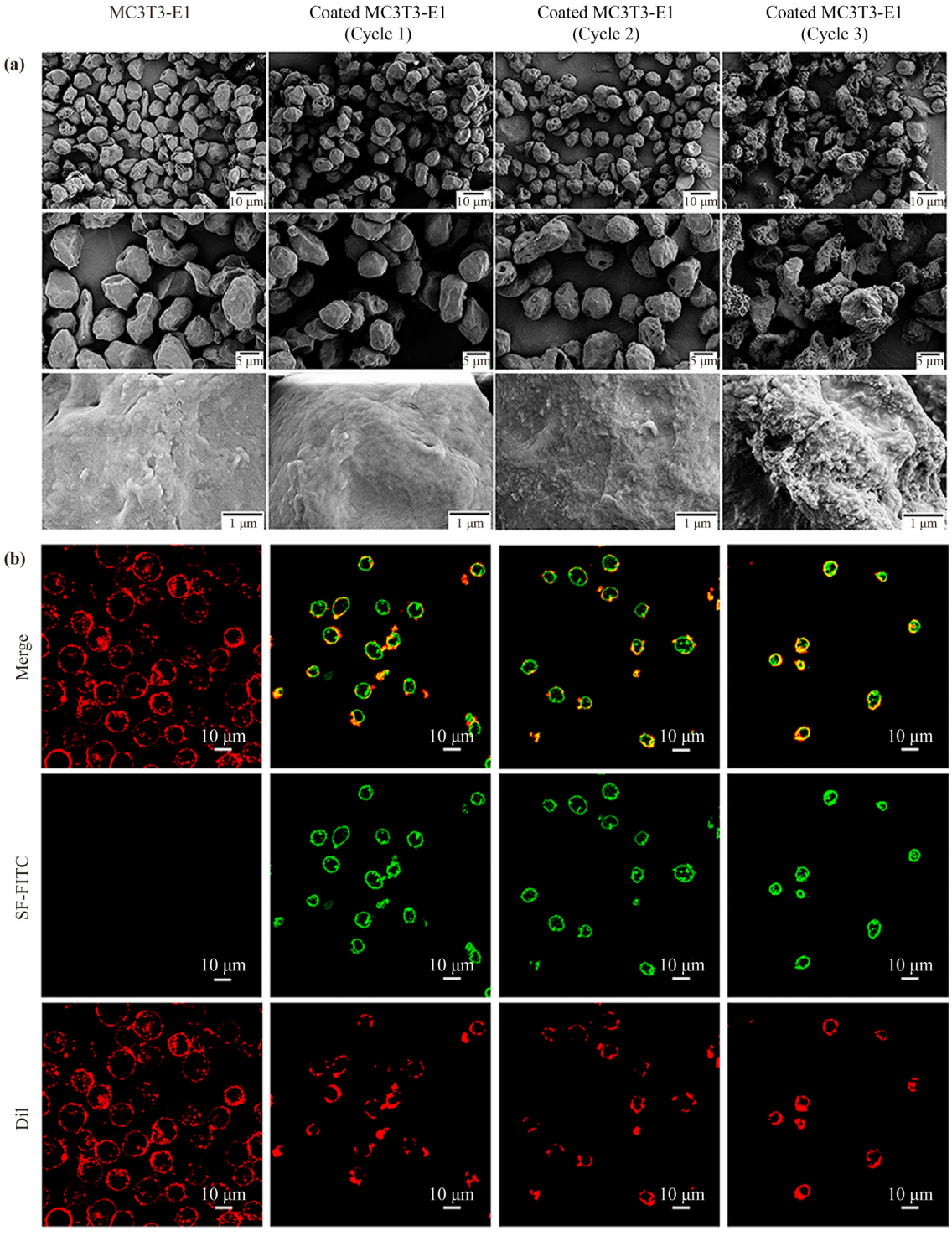

Fig. 3 (**a**) SEM observation and (**b**) CLSM observation of MC3T3-E1 and coating treated MC3T3-E1 cells. Green: SF-FITC, SF layer (labeled by FITC); red: cell membrane.

MC3T3-E1 cells in OS medium (MC3T3-E1 group), the coated cells' induction was further detected, and MC3T3-E1 cells cultured without the OS were used as a control as well. The actin network in cells plays an essential role in determining the overall shape of a cell by bridging integrins with the nucleus [44]. The coating treated MC3T3-E1 cells were cultured, and then the cytoskeleton was stained by rhodamine-conjugated phalloidin at 7 d. Figure 5(a) showed a comparable morphology with the MC3T3-E1 group and an apparent difference in the control group. The control group cells had osteoblasts-like morphology and were bipolar and elongated. In contrast,

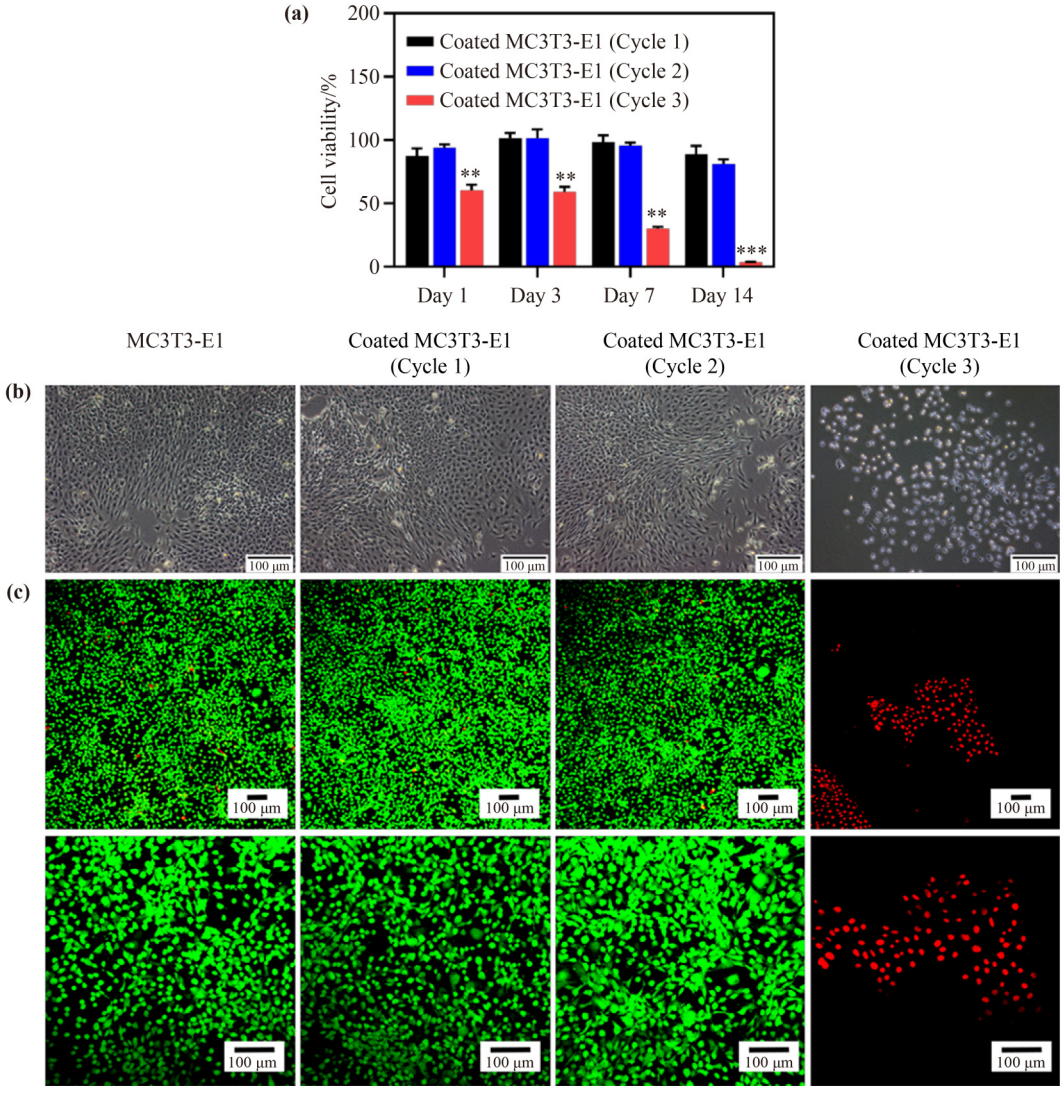

Fig. 4 Cell proliferation of MC3T3-E1 and coating treated MC3T3-E1 cells. (**a**) Cell viability of coating treated MC3T3-E1 cells after culture for 1, 3, 7, and 14 d. (**b**) Brightfield microscope observation and (**c**) live/dead staining images of MC3T3-E1 and coating treated MC3T3-E1 cells after culture for 14 d. Green: live cell; red: dead cell. The results are the mean ± SD of triplicate experiments, and statistical significance is analyzed as compared with the untreated MC3T3-E1 group: **, $p < 0.01$; ***, $p < 0.001$.

cells either with coating treatment or not (MC3T3-E1, coated MC3T3-E1 (Cycles 1 and 2)) displayed a polygonal shape in OS cultural medium (Fig. 5(a)). Based on this, the CLSM images indicated early osteogenic differentiation of the coating treated MC3T3-E1 cells.

Furthermore, morphological differences were measured with ImageJ software (Figs. 5(b)–5(e)). Marklein and co-workers reported that cell area and major/minor axis length are compelling indicators for osteogenic differentiation [45]. In this study, the mean cell area of coated MC3T3-E1 (Cycle 1, ~1645.31 μm^2; Cycle 2, ~1564.06 μm^2) significantly increased to ~1.6 times compared to the untreated cells (MC3T3-E1 group, ~1027.73 μm^2). Moreover, a significant difference in the major axis length (MC3T3-E1 group, ~67.31 μm; Cycle 1, ~44.98 μm; Cycle 2, ~52.75 μm) and a significant increasing minor axis length (MC3T3-E1 group, ~22.34 μm; Cycle 1, ~39.71 μm; Cycle 2, ~41.54 μm) were observed, which indicated cells differentiation towards osteocytes [46]. For the aspect ratio of cells, we also observed a substantial difference between the MC3T3-E1 group (~3.15) and the coating treated cells (Cycle 1, ~1.15; Cycle 2, ~1.29). It should be noted the increase of cell spread area induces osteogenic differentiation [47], and the morphology change from narrow to wide is associated with the differentiated stage of the cells [48–49], which suggested that the MC3T3-E1 may also shift their differentiation. Furthermore, in comparation

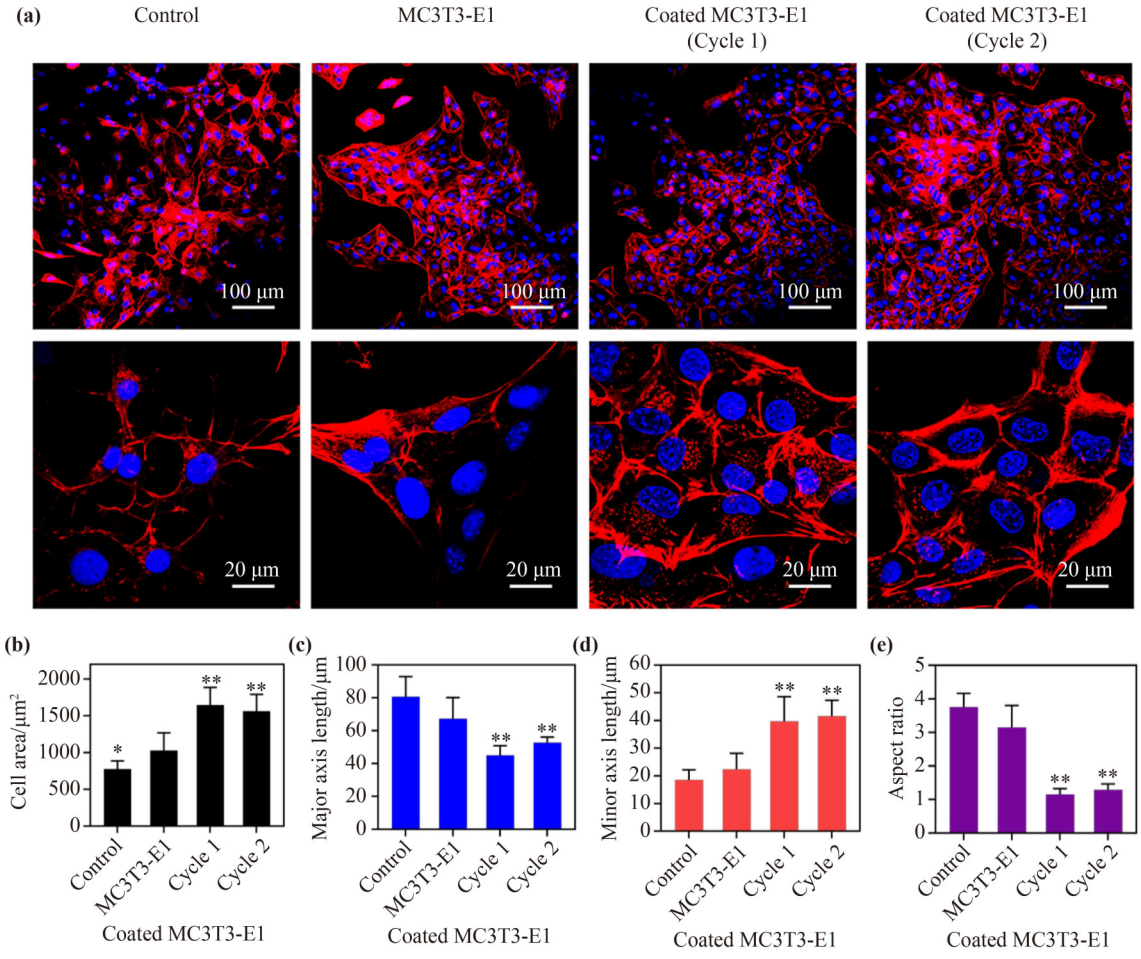

Fig. 5 Cell morphology of MC3T3-E1 and coating treated MC3T3-E1 cells after culture for 7 d. (**a**) Rhodamine-conjugated phalloidin (red) and DAPI (blue) staining images. Quantitative results of cell: (**b**) area, (**c**) major axis length, (**d**) minor axis length, and (**e**) aspect ratio. The statistical significance is analyzed as compared with the MC3T3-E1 group: *, $p < 0.05$; **, $p < 0.01$.

with the MC3T3-E1 group, the morphology transformation of coating treated MC3T3-E1 cells indicated an improved differentiation potential after the SF encapsulation.

Actually, the differentiation process is complex and multi-step that depends on the presence of specific bioactive factors and is affected by environmental cues [50]. Upregulation of ALP has been considered an essential indicator of osteogenic differentiation and bone formation, which is widely used to evaluate osteogenic differentiation [51–52]. Therefore, the effect of SF coating on the osteogenic differentiation of MC3T3-E1 was assessed by ALP activity assay. In the absence of an OS, MC3T3-E1 cells (control group) did not display upregulation of ALP activity as expected. In contrast, the presence of OS revealed positive upregulation of ALP activity for the other groups (Fig. 6(a)), which is similar to previous studies [53–54]. On Day 7, the coated MC3T3-E1 (Cycle 2) cells' activity reached significantly higher than the uncoated cells (MC3T3-E1 group). Furthermore, the coated MC3T3-E1 with Cycle 1 could dramatically increase compared with a similar level to the coated MC3T3-E1 (Cycle 2) group at 14 d. Notably, both were significantly higher than that of the uncoated cells (MC3T3-E1 group) and control ones (control group), indicating that SF coating of either MC3T3-E1 (Cycle 1) or MC3T3-E1 (Cycle 2) cells may present as a potential cue for osteogenic induction.

To further investigate the effect of SF coating on osteogenic differentiation at the genetic level, the following critical cytokines associated with osteocytes differentiation including ALP, Col I and OCN were further detected by qPCR after culturing cells for 14 d. As a marker for osteogenic differentiation, OCN is the most abundant bone-specific noncollagenous protein. We noted that the SF coating significantly promoted ALP and OCN expression for coated MC3T3-E1 cells (Fig. 6(b)) compared with the untreated MC3T3-E1 cells, which was

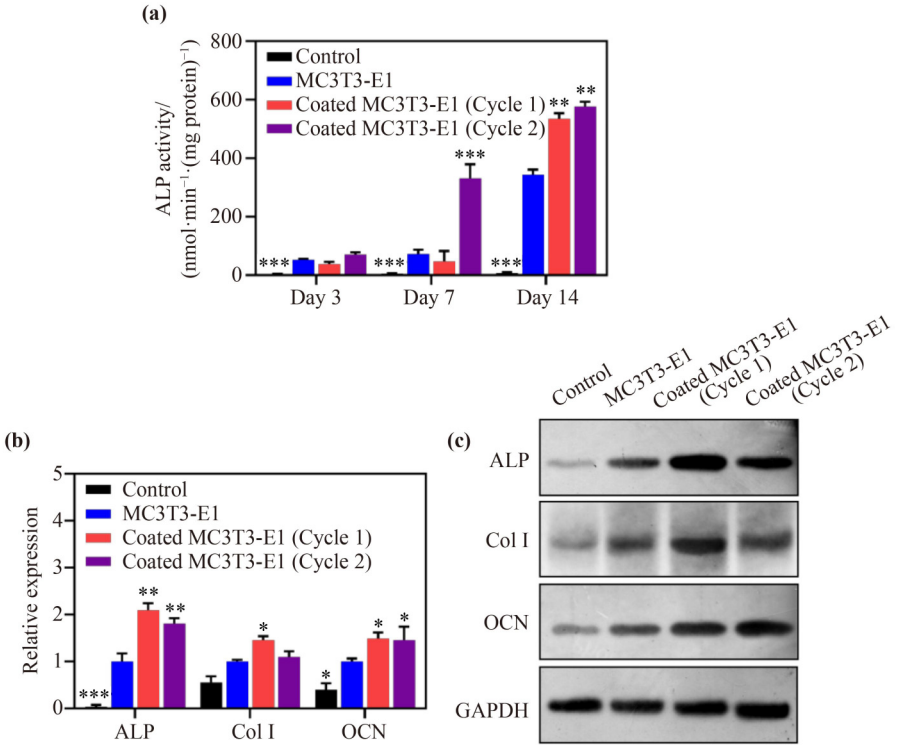

Fig. 6 Osteogenic differentiation of coating treated MC3T3-E1 cells. (**a**) ALP activity (normalized by the total protein content) of MC3T3-E1 and coating treated MC3T3-E1 cells after culture for 3, 7, and 14 d. Relative expression levels of (**b**) specific genes and (**c**) proteins for osteogenic differentiation. The results are the mean ± SD of triplicate experiments, statistical significance is analyzed as compared with the MC3T3-E1 group: *, $p < 0.05$; **, $p < 0.01$; ***, $p < 0.001$.

consistent with the ALP activity test. More generally, Col I, the most abundant protein in the bone matrix, is related to bone mineralization in the later stages of osteogenic differentiation, and upregulation of Col I was observed in coated MC3T3-E1 cells. Besides, western blotting was conducted to examine the expression of the proteins in the coated MC3T3-E1 cells (Fig. 6(c)). Again, the results confirmed that MC3T3-E1 cells with SF coating positively influenced osteogenic differentiation. These results demonstrated an analogous increased expression of ALP, Col I and OCN for SF-coated cells (Fig. 6(c)), which was in accordance with the qPCR test (Fig. 6(b)), indicating the great potential of osteocytes differentiation of the encapsulated osteoblasts.

3.4 Calcification of coating treated MC3T3-E1

Calcification is the typical sign during osteocytes differentiation. It is another critical osteogenic differentiation marker [55], which could be directly measured by calcium deposition using ARS staining [56]. Due to the upregulation of the specific proteins of osteogenesis (Fig. 6(c)), the mineralization induced by the cells may also be increased. The calcium deposits in the MC3T3-E1 cells formed were detected by ARS. As expected, according to the ARS staining, the red area implied that many mineralized nodules formed (Fig. 7(a)), and the area of nodules of the coated cells were significantly increased compared to the untreated cells (MC3T3-E1 group) (Fig. 7(b)), indicating the encapsulation may regulate the calcium mineralization of MC3T3-E1 cells [57–58]. These results suggested that the SF-based osteoblasts encapsulation may further be responsible for signal transduction of osteogenic differentiation and facilitate the calcium mineralization of MC3T3-E1 cells [32]. Additionally, the cell morphology is accordant with CLSM images (Fig. 5(a)), where a change in cell morphology from osteoblasts-like to osteocytes-like, further demonstrating a facile osteocytes modulation and mineralization via SF-based osteoblasts encapsulation.

Herein, we present an alternative strategy for integrating osteoblasts and SF by electrostatic layer-by-layer encapsulation, which expedited the osteoblasts towards osteocytes differentiation, rather than further optimizing complex processes and exogenous cytokines. Generally, cell behavior such as cell differentiation has been

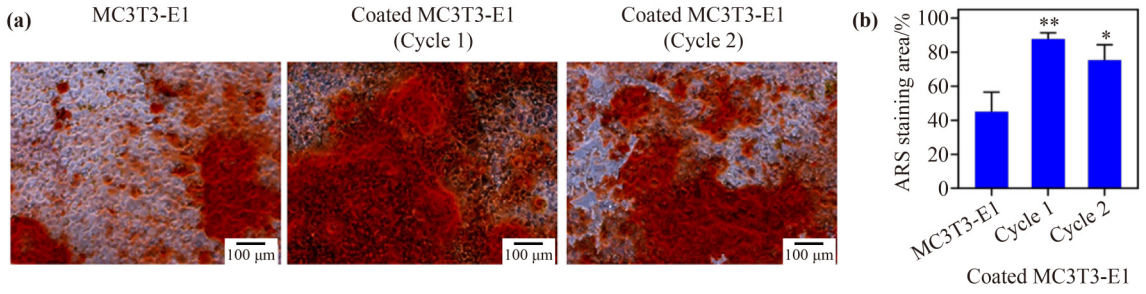

Fig. 7 ARS staining of MC3T3-E1 and coating treated MC3T3-E1 cells. (**a**) Brightfield microscopy observation images of MC3T3-E1 and coating treated MC3T3-E1 cells after culture for 21 d. (**b**) ARS staining area quantification of brightfield microscope observation images. The statistical significance is analyzed as compared with the MC3T3-E1 group: *, $p < 0.05$; **, $p < 0.01$.

promoted by the cytocompatible SF shell without using any other exogenous cytokines, revealing the alternative strategy for SF-based cell modification and reprogramming. More importantly, it should be noted that SF encapsulation provides an approach to establishing a stable and efficient method for SF-cell composites [57], which implies great potential for cell-hybrid materials therapeutics.

4 Conclusions

In summary, we presented a facile approach for encapsulating individual mammalian cells with SF. By rational coating treatments, these findings demonstrated that SF encapsulation not only has high biocompatibility but could be regarded as the cue to shift osteoblasts towards osteocytes, which suggested that the SF coating may provide a mimetic functional microenvironment for cell differentiation, implying their potential uses for single cell-materials engineering.

Disclosure of potential conflicts of interests The authors declare that they have no conflict of interest.

Acknowledgements This research was financially supported by the National Natural Science Foundation of China (Grant Nos. 51902289 and 51672250), the Natural Science Foundation of Zhejiang Province (Grant No. LQ19E020010), the Project of Zhejiang Provincial Department of Education (Grant No. Y201840323), the Key Project of Zhejiang Science and Technology (Grant Nos. 2021C01180 and 2019C04020), and the Research Foundation of ZSTU (Grant Nos. 18012134-Y and 2020Q008).

References

[1] Youn W, Kim J Y, Park J, et al. Single-cell nanoencapsulation: from passive to active shells. Advanced Materials, 2020, 32(35): 1907001

[2] Perry C C. Silicification: the processes by which organisms capture and mineralize silica. Reviews in Mineralogy and Geochemistry, 2003, 54(1): 291–327

[3] Hildebrand M, Lerch S J L. Diatom silica biomineralization: parallel development of approaches and understanding. Seminars in Cell & Developmental Biology, 2015, 46: 27–35

[4] Abdelhamid M A, Pack S P. Biomimetic and bioinspired silicifications: recent advances for biomaterial design and applications. Acta Biomaterialia, 2021, 120: 38–56

[5] Yao S, Jin B, Liu Z, et al. Biomineralization: from material tactics to biological strategy. Advanced Materials, 2017, 29(14): 1605903

[6] Liu Z, Xu X, Tang R. Improvement of biological organisms using functional material shells. Advanced Functional Materials, 2016, 26(12): 1862–1880

[7] Wang B, Liu P, Jiang W, et al. Yeast cells with an artificial mineral shell: protection and modification of living cells by biomimetic mineralization. Angewandte Chemie International Edition, 2008, 47: 3560–3564

[8] Wang G, Wang L, Liu P, et al. Extracellular silica nanocoat confers thermotolerance on individual cells: a case study of material-based functionalization of living cells. ChemBioChem, 2010, 11(17): 2368–2373

[9] Yang Y, Wang G, Zhu G, et al. The effect of amorphous calcium phosphate on protein protection against thermal denaturation. Chemical Communications, 2015, 51(41): 8705–8707

[10] Zhong D, Wang Y, Xie F, et al. A biomineralized Prussian blue nanotherapeutic for enhanced cancer photothermal therapy. Journal of Materials Chemistry B, 2022, 10(25): 4889–4896

[11] Amani H, Arzaghi H, Bayandori M, et al. Controlling cell behavior through the design of biomaterial surfaces: a focus on surface modification techniques. Advanced Materials Interfaces, 2019, 6(13): 1900572

[12] Zhao R, Cao J, Yang X, et al. Inorganic materials based macrophages regulation for cancer therapy: basic concepts and recent advances. Biomaterials Science, 2021, 9(13): 4568–4590

[13] Zhao R, Liu X, Yang X, et al. Nanomaterial-based organelles protect normal cells against chemotherapy-induced cytotoxicity. Advanced Materials, 2018, 30(27): 1801304

[14] Luo D, Ruan S, Liu A, et al. Laminin functionalized biomimetic apatite to regulate the adhesion and proliferation behaviors of neural stem cells. International Journal of Nanomedicine, 2018, 13: 6223–6233

[15] Xiong W, Zhao X, Zhu G, et al. Silicification-induced cell aggregation for the sustainable production of H_2 under aerobic conditions. Angewandte Chemie International Edition, 2015, 54(41): 11961–11965

[16] Youn W, Ko E H, Kim M H, et al. Cytoprotective encapsulation of individual jurkat T cells within durable TiO_2 shells for T-cell therapy. Angewandte Chemie International Edition, 2017, 56(36): 10702–10706

[17] Lee J, Choi J, Park J H, et al. Cytoprotective silica coating of individual mammalian cells through bioinspired silicification. Angewandte Chemie International Edition, 2014, 53(31): 8056–8059

[18] Wang Y, Zhong D, Xie F, et al. Manganese phosphate-doxorubicin-based nanomedicines using mimetic mineralization for cancer chemotherapy. ACS Biomaterials Science & Engineering, 2022, 8(5): 1930–1941

[19] Bhattarai D P, Shrestha S, Shrestha B K, et al. A controlled surface geometry of polyaniline doped titania nanotubes biointerface for accelerating MC3T3-E1 cells growth in bone tissue engineering. Chemical Engineering Journal, 2018, 350: 57–68

[20] Dirckx N, Moorer M C, Clemens T L, et al. The role of osteoblasts in energy homeostasis. Nature Reviews Endocrinology, 2019, 15(11): 651–665

[21] Khare D, Basu B, Dubey A K. Electrical stimulation and piezoelectric biomaterials for bone tissue engineering applications. Biomaterials, 2020, 258: 120280

[22] Abuna R P, Oliveira F S, Lopes H B, et al. The Wnt/β-catenin signaling pathway is regulated by titanium with nanotopography to induce osteoblast differentiation. Colloids and Surfaces B: Biointerfaces, 2019, 184: 110513

[23] Nadine S, Patrício S G, Correia C R, et al. Dynamic microfactories co-encapsulating osteoblastic and adipose-derived stromal cells for the biofabrication of bone units. Biofabrication, 2019, 12(1): 015005

[24] Cheng G, Davoudi Z, Xing X, et al. Advanced silk fibroin biomaterials for cartilage regeneration. ACS Biomaterials Science & Engineering, 2018, 4(8): 2704–2715

[25] DeBari M K, King C I III, Altgold T A, et al. Silk fibroin as a green material. ACS Biomaterials Science & Engineering, 2021, 7(8): 3530–3544

[26] Kundu B, Rajkhowa R, Kundu S C, et al. Silk fibroin biomaterials for tissue regenerations. Advanced Drug Delivery Reviews, 2013, 65(4): 457–470

[27] Asakura T, Tanaka T, Tanaka R. Advanced silk fibroin biomaterials and application to small-diameter silk vascular grafts. ACS Biomaterials Science & Engineering, 2019, 5(11): 5561–5577

[28] Zhang Y, Lu L, Chen Y, et al. Polydopamine modification of silk fibroin membranes significantly promotes their wound healing effect. Biomaterials Science, 2019, 7(12): 5232–5237

[29] Wang B, Xu H, Li J, et al. Degradable allyl *Antheraea pernyi* silk fibroin thermoresponsive hydrogels to support cell adhesion and growth. RSC Advances, 2021, 11(45): 28401–28409

[30] Mauney J R, Nguyen T, Gillen K, et al. Engineering adipose-like tissue *in vitro* and *in vivo* utilizing human bone marrow and adipose-derived mesenchymal stem cells with silk fibroin 3D scaffolds. Biomaterials, 2007, 28(35): 5280–5290

[31] Garcia-Fuentes M, Meinel A J, Hilbe M, et al. Silk fibroin/hyaluronan scaffolds for human mesenchymal stem cell culture in tissue engineering. Biomaterials, 2009, 30(28): 5068–5076

[32] Yan Y, Cheng B, Chen K, et al. Enhanced osteogenesis of bone marrow-derived mesenchymal stem cells by a functionalized silk fibroin hydrogel for bone defect repair. Advanced Healthcare Materials, 2019, 8(3): 1801043

[33] Kim D K, Lee S, Kim M, et al. Exosome-coated silk fibroin 3D-scaffold for inducing osteogenic differentiation of bone marrow derived mesenchymal stem cells. Chemical Engineering Journal, 2021, 406: 127080

[34] Luo D, Yao C, Zhang R, et al. Silk fibroin/collagen blended membrane fabricated via a green papermaking method for potential guided bone regeneration application: *in vitro* and *in vivo* evaluation. ACS Biomaterials Science & Engineering, 2021, 7(12): 5788–5797

[35] Kong H, Zhao R, Zhang Q, et al. Biosilicified oncolytic adenovirus for cancer viral gene therapy. Biomaterials Science, 2020, 8(19): 5317–5328

[36] Luo D, Xu X, Iqbal M Z, et al. siRNA-loaded hydroxyapatite nanoparticles for KRAS gene silencing in anti-pancreatic cancer therapy. Pharmaceutics, 2021, 13(9): 1428

[37] Iqbal M Z, Luo D, Akakuru O U, et al. Facile synthesis of biocompatible magnetic titania nanorods for T_1-magnetic resonance imaging and enhanced phototherapy of cancers. Journal of Materials Chemistry B, 2021, 9(33): 6623–6633

[38] Zhao R, Wang B, Yang X, et al. A drug-free tumor therapy strategy: cancer-cell-targeting calcification. Angewandte Chemie International Edition, 2016, 55(17): 5225–5229

[39] Buitrago J O, Patel K D, El-Fiqi A, et al. Silk fibroin/collagen

protein hybrid cell-encapsulating hydrogels with tunable gelation and improved physical and biological properties. Acta Biomaterialia, 2018, 69: 218–233

[40] Farina M, Alexander J F, Thekkedath U, et al. Cell encapsulation: overcoming barriers in cell transplantation in diabetes and beyond. Advanced Drug Delivery Reviews, 2019, 139: 92–115

[41] Chang L, Li X, Tang X, et al. Micro-patterned hydroxyapatite/silk fibroin coatings on Mg–Zn–Y–Nd–Zr alloys for better corrosion resistance and cell behavior guidance. Frontiers of Materials Science, 2020, 14(4): 413–425

[42] Xu S J, Cui F Z, Yu X L, et al. Glioma cell line proliferation controlled by different chemical functional groups *in vitro*. Frontiers of Materials Science, 2013, 7(1): 69–75

[43] Li D W, He F L, He J, et al. From 2D to 3D: the morphology, proliferation and differentiation of MC3T3-E1 on silk fibroin/chitosan matrices. Carbohydrate Polymers, 2017, 178: 69–77

[44] Chalut K J, Paluch E K. The actin cortex: a bridge between cell shape and function. Developmental Cell, 2016, 38(6): 571–573

[45] Marklein R A, Lo Surdo J L, Bellayr I H, et al. High content imaging of early morphological signatures predicts long term mineralization capacity of human mesenchymal stem cells upon osteogenic induction. Stem Cells, 2016, 34(4): 935–947

[46] Jhala D, Rather H, Vasita R. Polycaprolactone–chitosan nanofibers influence cell morphology to induce early osteogenic differentiation. Biomaterials Science, 2016, 4(11): 1584–1595

[47] Khan A U, Qu R, Fan T, et al. A glance on the role of actin in osteogenic and adipogenic differentiation of mesenchymal stem cells. Stem Cell Research & Therapy, 2020, 11(1): 283

[48] Rutkovskiy A, Stensløkken K O, Vaage I J. Osteoblast differentiation at a glance. Medical Science Monitor Basic Research, 2016, 22: 95–106

[49] Long E G, Buluk M, Gallagher M B, et al. Human mesenchymal stem cell morphology, migration, and differentiation on micro and nano-textured titanium. Bioactive Materials, 2019, 4: 249–255

[50] He L, Si G, Huang J, et al. Mechanical regulation of stem-cell differentiation by the stretch-activated Piezo channel. Nature, 2018, 555(7694): 103–106

[51] Yan R, Li J, Wu Q, et al. Trace element-augmented titanium implant with targeted angiogenesis and enhanced osseointegration in osteoporotic rats. Frontiers in Chemistry, 2022, 10: 839062

[52] Li M, Xiong P, Mo M, et al. Electrophoretic-deposited novel ternary silk fibroin/graphene oxide/hydroxyapatite nanocomposite coatings on titanium substrate for orthopedic applications. Frontiers of Materials Science, 2016, 10(3): 270–280

[53] Liu C, Zhai H, Zhang Z, et al. Cells recognize and prefer bone-like hydroxyapatite: biochemical understanding of ultrathin mineral platelets in bone. ACS Applied Materials & Interfaces, 2016, 8(44): 29997–30004

[54] Yu Y, Sun B, Yi C, et al. Stem cell homing-based tissue engineering using bioactive materials. Frontiers of Materials Science, 2017, 11(2): 93–105

[55] Tang Y, Rajendran P, Veeraraghavan V P, et al. Osteogenic differentiation and mineralization potential of zinc oxide nanoparticles from *Scutellaria baicalensis* on human osteoblast-like MG-63 cells. Materials Science and Engineering C, 2021, 119: 111656

[56] Patel M, Koh W G. Composite hydrogel of methacrylated hyaluronic acid and fragmented polycaprolactone nanofiber for osteogenic differentiation of adipose-derived stem cells. Pharmaceutics, 2020, 12(9): 902

[57] Karaji Z G, Jahanmard F, Mirzaei A H, et al. A multifunctional silk coating on additively manufactured porous titanium to prevent implant-associated infection and stimulate bone regeneration. Biomedical Materials, 2020, 15(6): 065016

[58] Melke J, Midha S, Ghosh S, et al. Silk fibroin as biomaterial for bone tissue engineering. Acta Biomaterialia, 2016, 31: 1–16